

The Cytotoxicity of Phenolic Sesquiterpenes from *Dysoxylum parasiticum* Leaves Against MCF-7 Human Breast Cancer Cells

Ferry Ferdiansyah Sofian^{1,2,3*}, Amrina Virliana¹, Ahda Salsabila Izzaturrahmi¹, Ellin Febrina⁴, Eri Bachtiar⁵, Tjandrawati Mozef⁶, Aiyi Asnawi⁷, Kindi Farabi^{3,8}, Nurlelasari Nurlelasari⁸, Yasmiwar Susilawati^{1,2}, Anas Subarnas⁴, Unang Supratman^{3,8}, and Yoshihito Shiono⁹

¹Department of Pharmaceutical Biology, Faculty of Pharmacy, Universitas Padjadjaran, Jl. Raya Bandung-Sumedang Km. 21, Jatinangor, Sumedang 45363, Indonesia

²Study Center of Herb, Faculty of Pharmacy, Universitas Padjadjaran, Jl. Raya Bandung-Sumedang Km. 21, Jatinangor, Sumedang 45363, Indonesia

³Central Laboratory of Universitas Padjadjaran, Jl. Raya Bandung-Sumedang Km. 21, Jatinangor, Sumedang 45363, Indonesia

⁴Department of Pharmacology and Clinical Pharmacy, Faculty of Pharmacy, Universitas Padjadjaran, Jl. Raya Bandung-Sumedang Km. 21, Jatinangor, Sumedang 45363, Indonesia

⁵Department of Marine Science, Faculty of Fishery and Marine Science, Universitas Padjadjaran, Jl. Raya Bandung-Sumedang Km. 21, Jatinangor, Sumedang 45363, Indonesia

⁶Research Center for Pharmaceutical Ingredients and Traditional Medicine, National Research and Innovation Agency (BRIN), Jl. Raya Bogor Km. 46, Cibinong 16911, Indonesia

⁷Department of Pharmacochimistry, Faculty of Pharmacy, Universitas Bhakti Kencana, Jl. Soekarno-Hatta No. 754, Bandung 40617, Indonesia

⁸Department of Chemistry, Faculty of Mathematics and Natural Sciences, Universitas Padjadjaran, Jl. Raya Bandung-Sumedang Km. 21, Jatinangor, Sumedang 45363, Indonesia

⁹Department of Food, Life, and Environmental Science, Faculty of Agriculture, Yamagata University, 1-23 Wakaba-machi, Tsuruoka City, Yamagata 997-8555, Japan

* **Corresponding author:**

email: ferry.ferdiansyah@unpad.ac.id

Received: August 23, 2025

Accepted: January 15, 2026

DOI: 10.22146/ijc.110617

Abstract: The sesquiterpene phenols from *Dysoxylum parasiticum* leaves have received limited study, particularly regarding their mechanisms of action against breast cancer and their associated molecular targets. Thus, this study isolated bioactive secondary metabolites from *D. parasiticum* leaves and evaluated their cytotoxicity and molecular interactions with breast cancer targets. Two previously characterized sesquiterpene phenol derivatives, dysoxyphenol (**1**) and 7-hydroxycalamenene (**2**), were isolated from *D. parasiticum* leaf extracts. The chemical characterization was established through comprehensive spectral analyses and confirmed by optical rotation data. Cytotoxic evaluation demonstrated notable bioactivity against MCF-7 cells, with half-maximal inhibitory concentrations of 196.02 and 94.44 μM for compounds **1** and **2**, respectively. Computationally, molecular docking and molecular dynamics simulations revealed that both compounds **1** and **2** exhibit stable interactions with a breast cancer-human estrogen receptor (PDB ID: 3ERT). The results suggest that these findings contribute to understanding the anticancer potential of sesquiterpene phenol derivatives from *D. parasiticum*, making them promising candidates for developing novel cancer drugs.

Keywords: sesquiterpene phenols; *Dysoxylum parasiticum*; Meliaceae; cytotoxicity; MCF-7 cells

■ INTRODUCTION

The challenges associated with the discovery and development of new anticancer drugs are worldwide issues that necessitate the investigation of natural resources as viable alternatives [1]. Plants have recently made important contributions to the discovery of bioactive substances with potential as new therapeutic candidates [2]. *Dysoxylum parasiticum* (Osbeck) Kosterm., a Meliaceae species within the genus *Dysoxylum*, thrives in tropical to subtropical regions [3]. In Indonesia, it occurs in West Java, including the Pangandaran area, where it is part of the diet of the Javan langur (*Trachypithecus auratus sondaicus*) [4-5]. The tendency of primates to self-medicate by consuming specific plants (zoopharmacognosy) suggests a notable phytochemical potential in these taxa [6]. Studies of primate-consumed plants from Pangandaran, including *D. parasiticum*, have revealed antibacterial [7], antiplasmodial, and antitoxoplasma activities [8]. The stem bark and leaves of *D. parasiticum* contain a variety of bioactive compounds, such as sesquiterpenoids [9-11], limonoids [12], and a trinorditerpenoid [13], which have been shown to have immunomodulatory effects on human and murine cells, antidiabetic and antioxidant activities as well as cytotoxic activities against several cancer cell lines [10-13].

In accordance with those considerations, the objective of this investigation focuses on purifying and determining the structure of phenolic sesquiterpene metabolites found in *D. parasiticum* leaves. Moreover, the cytotoxicity of these metabolites against MCF-7 human mammary carcinoma cells is assessed to explore their therapeutic potential in cancer treatment. The assessment was further validated using *in silico* analyses, including molecular docking and molecular dynamics (MD) simulations, focused on a key receptor implicated in breast cancer progression. This study not only enhances understanding of the chemical constituents and bioactivity of *D. parasiticum* but also provides a novel, deeper understanding of the structure-activity relationships of phenolic sesquiterpene compounds as potential anticancer agents and validates the ethnopharmacological approach based on observations of

primate feeding behavior in the discovery of natural medicinal products.

■ EXPERIMENTAL SECTION

Materials

Fresh leaves of *D. parasiticum* (Osbeck) Kosterm. were collected in August 2017 from the Pangandaran Nature Reserve, West Java, Indonesia. The specimen was authenticated by Mr. Joko Kusmoro (Laboratory of Plant Taxonomy, Department of Biology, Universitas Padjadjaran) under identification number 426/HB/08/2017. A voucher sample was deposited at the Herbal Research Center, Universitas Padjadjaran, with archive code PM-002.

Instrumentation

Optical rotation was measured on a SEPA-300 polarimeter. The ultraviolet (UV), Fourier-transform infrared (FTIR), and electronic circular dichroism (ECD) spectra were obtained employing a Shimadzu UV mini-1240 (Shimadzu, Japan), Horiba FT710 (Horiba, Japan), and Jasco J-20A automatic recording spectropolarimeters (Jasco, Japan), respectively. The JEOL JMS-700 (JEOL, Japan) instrument was used to obtain mass spectra. Nuclear magnetic resonance (NMR) spectral data were acquired on a JEOL ECZ-600 (JEOL, Japan). The chemical shifts (δ , ppm) were recorded in CDCl_3 with tetramethylsilane as the internal reference. Standard JEOL pulse sequences were employed to acquire spectra, including ^1H -NMR at 600 MHz, ^{13}C -NMR at 150 MHz, along with heteronuclear multiple quantum coherence (HMQC), heteronuclear multiple-bond coherence (HMBC), ^1H - ^1H correlated spectroscopy (COSY), and nuclear overhauser effect (NOE) analyses.

For chromatography, silica gel 60 (Merck, Germany) and octadecylsilane (ODS; Fuji Silysia, Japan) were employed. Semi-preparative HPLC separations used a Waters Alliance e2695A system with a 2489 UV-vis detector set at 257 nm (Waters Corporation, Milford, MA, USA) on a reverse-phase HPLC C18 column (Agilent Zorbax Eclipse Plus C18, 5 μm , 4.6 I.D. \times 250 mm) (Agilent Technologies, Inc., Santa Clara, CA, USA). Thin-layer chromatography (TLC) analysis was executed on precoated silica gel 60 F₂₅₄ plates (Merck, Germany).

Compound visualization was performed under UV light (254 and 365 nm) and followed by treatment with 10% vanillin (Merck, Germany) in H₂SO₄ spray reagent.

Procedure

Extraction and isolation

The leaves were sorted, rinsed with tap water, and held at 40 °C during transport. The material was then air-dried at ambient temperature (1.39 kg, 25 °C) for 5 days and extracted with 15 L of 95% ethanol (EtOH) three times in 24 h at 25 °C. Subsequently, a constant mass of viscous extract (143.32 g) was obtained by evaporating the solvent at 40–50 °C. Then, the EtOH extract (143.32 g) was dispersed in 1 L of demineralized water (H₂O) and subsequently partitioned with *n*-hexane, yielding the *n*-hexane-soluble fraction. The *n*-hexane fraction (50.94 g) was subjected to silica gel column separation employing a gradient progressive elution with *n*-hexane and ethyl acetate (EtOAc; 100:0–0:100, 10%, v/v; each 600 mL) to afford 11 fractions (Frs. 1–1 to 1–11). Fractions 1–3 (23.85 g; 20% *n*-hexane–EtOAc) were subsequently purified using a progressive *n*-hexane–chloroform (CHCl₃; 100:0–0:100, 5%, v/v; each 300 mL) gradient system, producing 22 fractions (Frs. 1–3-1 to 1–3-22). All fractions were monitored by the TLC using vanillin–H₂SO₄ as the staining reagent. The appearance of a characteristic light blue coloration indicated the presence of the target compound(s). Fractions 1–3-8 to 1–3-12 (9.42 g) were subsequently fractionated through open column chromatography using silica gel with isocratic *n*-hexane–EtOAc (30:1, v/v; each 120 mL) elution, resulting in 19 combined subfractions (Frs. 1–3-8.12-1 to 1–3-8.12-19). Subfraction 1–3-8.12-9 (1.05 g) was separated with an ODS column using an isocratic elution of H₂O–methanol (MeOH; 1:9, v/v; each 20 mL) to afford four combined fractions (Frs. B1–3-8.12-9.1 to B1–3-8.12-9.4). Fraction B1–3-8.12-9.2 (254.3 mg) underwent additional purification via semi-preparative HPLC (1.0 mL/min flow rate) employing a H₂O–MeOH gradient system (35:65–15:85, v/v), yielding compounds **1** (12.8 mg, *t_R* = 17.3 min) and **2** (5.6 mg, *t_R* = 18.6 min) (Fig. S1).

Spectroscopic data

Dysoxyphenol (1). Yellowish oil; [α]_D²³ +14° (c 0.12, CHCl₃);

UV λ_{\max} (MeOH) nm (log ϵ): 207.5 (4.4), 225.5 (3.8) and 282 (3.3); ECD (MeOH) λ_{\max} ($\Delta\epsilon$) 202 (–4.1), 214.5 (+1.3), 232.5 (–0.3), 282 (–0.6) nm; FTIR ν_{\max} (KBr) cm^{–1}: 3389, 2952, 2352, 1712, 1515, 1465; ¹H-NMR (600 MHz, in CDCl₃) and ¹³C-NMR (150 MHz, in CDCl₃) spectral assignments, detailed in Table 1; HR-ESI TOF-MS *m/z* [M+H]⁺: 219.1743, calculated for C₁₅H₂₃O, 219.1749. The spectroscopic data are presented in Fig. S2–S12.

7-Hydroxycalamenene (2). Yellowish oil; [α]_D²³ +46° (c 0.06, CHCl₃); UV λ_{\max} (MeOH) nm (log ϵ): 207 (4.3), 226.5 (3.8) and 282 (3.3); FTIR ν_{\max} (KBr) cm^{–1}: 3442, 2936, 2344, 1709, 1528, 1475; ¹H-NMR (600 MHz, in CDCl₃) and ¹³C-NMR (150 MHz, in CDCl₃) spectral assignments, detailed in Table 1. The spectroscopic data are presented in Fig. S13–S21.

ECD experiment and calculations

A sample was prepared for the ECD experiment at a concentration of 25 μ g/mL in MeOH. The measurement was recorded over the range 200–400 nm at 25 °C, with solvent (blank) subtraction to improve signal-to-noise. To refine the absolute stereochemical assignment of **1**, we employed a computational workflow combining gas-phase density functional theory (DFT) and time-dependent DFT (TD-DFT) calculations using Gaussian 09 [14–15]. Conformational sampling was first performed with GMMX [16] under the MMFF94 force field, yielding eight conformers of **1a**, as shown in Fig. S22 and Table S1. These structures were geometry-optimized at the ω B97X-D/6-31G(d) level in Gaussian 09, and harmonic vibrational frequency analyses were used to confirm each as a true energy minimum rather than a transition state, guaranteeing reliable conformers for subsequent TD-DFT calculations [17]. These ECD spectra were then computed via TD-DFT at the ω B97X-D/6-31G(d) gas-phase level. For each conformer, simulated ECD spectra were generated using Gaussian broadening (half-bandwidth 0.36 eV), and the overall ECD profile was obtained as a Boltzmann-weighted sum reflecting the relative conformer populations. For the assignment of absolute configuration, the experimental ECD spectrum of **1** was compared with the calculated ECD spectrum of **1a**.

Cell culture and cytotoxic assay

Cell cultivation of MCF-7 (ATCC HTB-22, Manassas, VA, USA) was performed at 37 °C in a 5% CO₂ humidified incubator using RPMI-1640 culture medium (Gibco, Cat. No. 11875-093, Life Technologies Corp., USA) and enhanced with 10% heat-treated FBS (Gibco, Cat. No. 10270-106, Life Technologies Corp., USA) and 1% of combined solution of penicillin (100 U/mL) and streptomycin (10 µg/mL) (BioReagent, Cat. No. P4333, Sigma-Aldrich Corp., USA). Cell viability was assayed using resazurin sodium salt (BioReagent, Cat. No. R7017, Sigma-Aldrich Corp., USA) after a 24-h incubation period and quantified at 570 nm. Then, the cytotoxicity of **1** and **2** was measured by resazurin reduction assay using the described method [9], with cisplatin (EDQM, Strasbourg, France) as a positive control. The IC₅₀ values were calculated using GraphPad Prism 10.0 (GraphPad Software, Inc., San Diego, CA, USA). The tools perform data fitting by assuming that the response curve follows a symmetrical sigmoidal shape using a four-parameter logistic regression model (this value is also referred to as the relative IC₅₀ parameter), as in Eq. (1) [18].

$$Y = Y_{\min} + \frac{Y_{\max} - Y_{\min}}{1 + \left(\frac{X}{IC_{50}}\right)^{\text{Hill coefficient}}} \quad (1)$$

Molecular docking study

Ligand preparation. The chemical structures of **1** and **2** were downloaded from the PubChem database (<https://pubchem.ncbi.nlm.nih.gov>; accessed on 20 June 2025) in *.sdf format. These structures were processed and optimized using Avogadro (version 1.2.0, <https://avogadro.cc>) [19], a molecular visualization and editing software. Avogadro allows conversion of *.sdf files to a more usable format for molecular docking simulations, specifically *.pdb, which is compatible with AutoDock4.2.6 and other simulation tools. Next, geometry optimization was performed using the MMFF94 force field in Avogadro to ensure the ligands were in their lowest-energy conformation. Geometry optimization is a crucial step in molecular modeling, as it allows ligands to adopt their most stable 3D structures, thereby improving the accuracy of subsequent docking simulations. The MMFF94 force field was chosen because it is well-suited for organic molecules, offering a good

balance between computational efficiency and accuracy [20]. After this optimization, the ligands were ready for further analysis and docking simulations, ensuring that their 3D structures were energetically favorable and geometrically accurate for interaction with the protein targets.

Macromolecule preparation. The crystal structure of the estrogen receptor alpha (PDB ID: 3ERT), resolved at 1.90 Å, was obtained from the RCSB Protein Data Bank (www.rcsb.org; accessed on 20 June 2025). Protein selection was determined by its relevance to breast cancer biology and its established role in ligand–receptor interactions within oncogenic pathways. The structure was downloaded in *.pdb format, which is widely used in molecular modeling as it provides detailed information on atomic coordinates, chain identifiers, and structural components of macromolecules. Following retrieval, the protein structure was subjected to a cleaning process to remove non-essential molecules, including water, co-crystallized solvents, and heteroatoms, while retaining only the core macromolecule and its native ligand (4-hydroxytamoxifen; code: OHT). This step was critical for eliminating potential sources of interference and ensuring a clean binding environment for molecular docking simulations. The cleaned structure was then saved in *.pdb format and prepared for docking by adding polar hydrogen and assigning appropriate partial charges. These modifications are essential for accurate modeling of intermolecular interactions, particularly hydrogen bonding and electrostatic forces, during docking analysis. This careful preparation ensured that the target protein was optimized for reliable and meaningful interaction studies with the candidate ligands.

Molecular docking simulation. Molecular docking simulations were performed using AutoDock 4.2 [21] to evaluate the binding interactions of compounds **1** and **2** with the estrogen receptor alpha protein target (PDB ID: 3ERT). The docking protocol was validated by redocking the native ligand, OHT, into its crystallographic binding site on the estrogen receptor alpha, and evaluating the root-mean-square deviation (RMSD) between the predicted and experimental poses. An RMSD ≤ 2.0 Å was taken as evidence of an acceptable protocol [22]. For

docking, the grid box was set to $40 \times 40 \times 40$ points, with a spacing of 0.375 Å, encompassing the target protein's active site. Using parameters optimized during validation, docking simulations were performed for compounds **1** and **2**. Binding affinities, docking scores, and interaction profiles were then analyzed using AutoDockTools version 1.5.6 and Discovery Studio Visualizer version 2019 to identify key molecular interactions, supporting the evaluation of these compounds as potential therapeutic agents for breast cancer.

MD simulation. The GROMACS software package (version 2023.1) was employed for MD simulations to examine the stability and dynamic properties of the protein–ligand complexes [23–24]. Simulations were performed over 100 ns on a high-performance workstation equipped with an Intel Xeon E5-2690 V3 central processing unit, 32 GB of RAM, and an NVIDIA RTX 3060 graphics processing unit. The best docking poses of the native ligand and compounds **1** and **2** were used as initial structures for MD simulations. Each ligand was positioned in the estrogen receptor alpha binding site to evaluate its time-dependent interactions in a realistic biological environment. The molecular systems were immersed in cubic aqueous boxes, charge-balanced through appropriate counterions, and subjected to energy minimization to eliminate unfavorable interactions and improve structural geometry. In the following, each system was equilibrated and then simulated at constant temperature and pressure (NPT ensemble) with periodic boundary conditions. Throughout the simulation, key parameters, including root-mean-square fluctuation (RMSF), binding energy, and RMSD, were monitored. These metrics provided insights into the conformational stability of the protein–ligand complexes and the persistence of interactions over time, aiding in the assessment of compounds **1** and **2** as drug candidates.

Data visualization. Visualization and analysis of the docking and MD simulation data were performed using various computational tools to enhance clarity and interpretability. Docking results, including binding energies and predicted inhibition constants (K_i) for compounds **1** and **2** in complex with the estrogen receptor alpha (PDB ID 3ERT), were organized in a table to clearly

present and facilitate direct comparison of their binding performance. To further explore ligand–receptor interactions, Discovery Studio Visualizer was used to examine key non-covalent forces including hydrogen bonding, hydrophobic interactions, and π – π stacking. These visualizations provided valuable context for interpreting docking poses and identifying critical residues involved in binding [25]. For MD simulations, Python version 3.11 was employed to generate RMSD plots, which tracked the structural stability of each complex over the 100 ns simulation, and RMSF plots, which highlighted the flexibility of specific amino acid residues. These dynamic visualizations complemented the static docking data by revealing how well each ligand maintained its binding pose under physiological conditions. Taken together, the graphical and tabular analyses provided a comprehensive overview of the performance of compounds **1** and **2** in both docking and MD simulations, reinforcing their potential as promising lead compounds in the development of breast cancer therapeutics.

■ RESULTS AND DISCUSSION

Structure Elucidation of Isolated Compounds

Two known sesquiterpene phenols, dysoxyphenol (**1**) [11,26] and (+)-(1*S*,4*R*)-7-hydroxycalamenene (**2**) [27] were isolated from the leaf extracts of *D. parasiticum*, which were obtained by maceration in EtOH at 25 °C. Elucidation of compounds **1** and **2** structures was achieved through comprehensive analysis of their spectral and physicochemical properties data, including high-resolution electrospray ionization time-of-flight mass spectrometry (HR-ESI TOF-MS), UV, FTIR, 1D and 2D NMR analyses, as well as optical rotation measurement, all of which were consistent with previously reported literature values (Fig. 1). Additionally, the precise absolute stereochemical configuration of compound **1** was established using ECD spectroscopic method.

Compound **1** ($[\alpha]_D^{23} +14^\circ$) was identified as a yellowish oil. According to HR-ESI TOF-MS, the ion peak at m/z 219.1743 $[M+H]^+$ corresponded to compound **1**, which has a molecular formula $C_{15}H_{22}O$ with

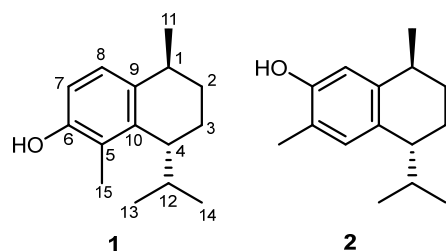


Fig 1. Structures of compounds **1** and **2**

five degrees of unsaturation (calculated for $C_{15}H_{23}O$, 219.1749). The UV spectrum exhibited maxima at 207.5, 225.5, and 282 nm, indicative of an aromatic system and particularly suggesting the presence of phenolic compounds. The FTIR spectrum displayed characteristic absorptions corresponding to hydroxy groups at 3389 cm^{-1} and benzene ring vibrations at 1515 and 1465 cm^{-1} , confirming their presence in the structure. The $^1\text{H-NMR}$ spectrum measured in CDCl_3 (Table 1) exhibited two aromatic doublet signals at δ_{H} 6.95 (H-8) and 6.62 (H-7), each with a coupling constant of 8.3 Hz. These features indicate the presence of a pair of *ortho*-coupled aromatic protons; a phenolic hydroxyl proton at δ_{H} 4.52 (6-OH); three aliphatic methine protons at δ_{H} 2.94 (H-4), 2.72 (H-

1), and 1.95 (H-12); an olefinic methyl singlet at δ_{H} 2.19 (H-15); three methyl doublets at δ_{H} 1.23 (H-11), 0.88 (H-14), and 0.79 (H-13); and other aliphatic protons attributed to two methylenes [δ_{H} 1.94 and 1.23 (H-2); δ_{H} 1.83 and 1.74 (H-3)]. The $^{13}\text{C-NMR}$ spectrum (Table 1) exhibited 15 carbon resonances, including 6 sp^2 and 9 sp^3 carbons, indicative of an aromatized structure of **1**. The long-range correlations from the phenolic hydroxyl proton to C-5, C-6, and C-7 and from H₃-15 to C-5, C-6, and C-10 were observed in the HMBC spectral data (Table S2 and Fig. 2), indicating that the phenolic hydroxyl (6-OH) and the quaternary aromatic methyl (CH_3 -15) groups could be at C-6 and C-5, respectively. Moreover, the two aromatic doublets H-7 and H-8 with $J_{7,8} = 8.3\text{ Hz}$ showed the $^1\text{H-}^1\text{H}$ COSY correlation of H-7/H-8 coupled and HMBC correlations from H-7 to C-5, C-6, and C-9 and from H-8 to C-1, C-6, and C-10 (Fig. 2). These results inferred the presence of a 5,6,9,10-tetrasubstituted aromatic ring. In addition, the $^1\text{H-}^1\text{H}$ COSY correlations of H₃-13/H-12/H-4/H₂-3/H₂-2/H-1/H₃-11 and H-12/H₃-14 indicated a $\text{CH}(\text{Me})\text{CH}_2\text{CH}_2\text{CHCH}(\text{Me})_2$ spin system as for **1** and

Table 1. ^1H (600 MHz) and ^{13}C (150 MHz) NMR data for **1** and **2** in CDCl_3

Position	Compound 1		Compound 2	
	δ_{C} , type	δ_{H} , mult. (J in Hz)	δ_{C} , type	δ_{H} , mult. (J in Hz)
1	31.6, CH	2.72, sext (6.8)	32.7, CH	2.71, sext (6.8)
2	29.6, CH_2	1.95, <i>m</i>	30.9, CH_2	1.93, <i>m</i>
		1.23, <i>m</i>		1.31, <i>m</i>
3	21.9, CH_2	1.83, <i>m</i>	21.7, CH_2	1.80, <i>m</i>
		1.74, <i>m</i>		1.54, <i>m</i>
4	40.9, CH	2.94, <i>td</i> (4.4, 6.7)	43.2, CH	2.63, <i>q</i> (6.1)
5	121.7, C		130.6, CH	6.94, <i>s</i>
6	151.9, C		120.7, C	
7	112.1, CH	6.62, <i>d</i> (8.3)	151.5, C	
8	124.2, CH	6.95, <i>d</i> (8.3)	113.1, CH	6.65, <i>s</i>
9	136.1, C		142.3, C	
10	141.3, C		132.4, C	
11	22.3, CH_3	1.23, <i>d</i> (6.8)	22.4, CH_3	1.24, <i>d</i> (6.9)
12	31.9, CH	1.95, <i>m</i>	32.0, CH	2.21, <i>m</i>
13	19.2, CH_3	0.79, <i>d</i> (6.7)	17.3, CH_3	0.70, <i>d</i> (6.8)
14	21.3, CH_3	0.88, <i>d</i> (6.8)	21.3, CH_3	0.99, <i>d</i> (6.8)
15	12.5, CH_3	2.19, <i>s</i>	15.7, CH_3	2.21, <i>s</i>
6-OH		4.52, <i>s</i>		
7-OH				4.47, <i>s</i>

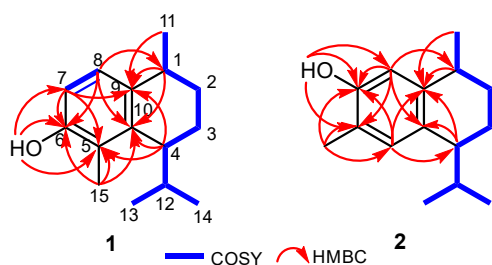


Fig 2. ^1H - ^1H COSY (blue bold lines) and selected HMBC (red arrows) correlations of compounds **1** and **2**

and the HMBC correlations from H-3 to C-5, C-9, and C-10 and from H-6 to C-8, C-9, and C-10 showed that the C-4 and C-1 were linked to aromatic ring on the C-10 and C9, respectively (Fig. 2). These HMBC correlations suggested the existence of a 3,4,5,6-tetrahydronaphthalen structure with methyl substitution on the position of C-1 and C-5 and isopropyl substitution on the position of C-4. Significant NOE correlations of H-4/H₃-15, H-1/H₃-12, and H-1/H₃-13 indicated that 5-CH₃ (C-15) and H-4 existed in the equatorial position, and both 1-CH₃ and the 4-isopropyl groups revealed a *trans* relationship (Fig. 3). The positive optical rotation ($[\alpha]_D^{23} +14^\circ$) of **1** was identical to dysoxyphenol ($[\alpha]_D^{25} +34^\circ$) [26], but it was not a similar value. Accordingly, ECD analysis established the absolute configuration of compound **1**, as shown in Fig. 1. Comparison between the ECD spectrum of **1** [ECD (MeOH) λ_{max} ($\Delta\epsilon$) 202 (-4.1), 214.5 (+1.3), 232.5 (-0.3), 282 (-0.6) nm] and TD-DFT calculations for **1a** at the wB97XD/6-31G(d) level was performed. The calculated

ECD spectrum of the enantiomeric form of **1a** showed strong concordance with the observed experimental spectrum (Fig. 4). This demonstrated that the absolute stereochemical configurations at C-1 and C-4 in **1** were 1*S* and 4*R*, respectively. Thus, the absolute structure of **1** was determined as (1*S*,4*R*)-4-isopropyl-1,5-dimethyl-1,2,3,4-tetrahydronaphthalen-6-ol as shown in Fig. 1. Spectroscopic data comparison, especially NMR data of **1** with dysoxyphenol isolated from *D. densiflorum* seeds [26] revealed that those two compounds were identical. Thus, compound **1** is present as dysoxyphenol that was first isolated in those *D. densiflorum* seeds.

Compound **2** was characterized as an optically active yellowish oil with an $[\alpha]_D^{23}$ value of $+46^\circ$. UV spectroscopic analysis revealed characteristic absorption bands at 207, 226, and 282 nm, providing strong evidence

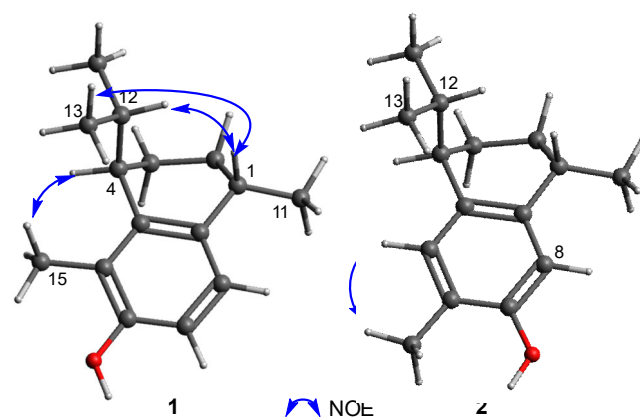


Fig 3. Key NOE correlations of compounds **1** and **2**

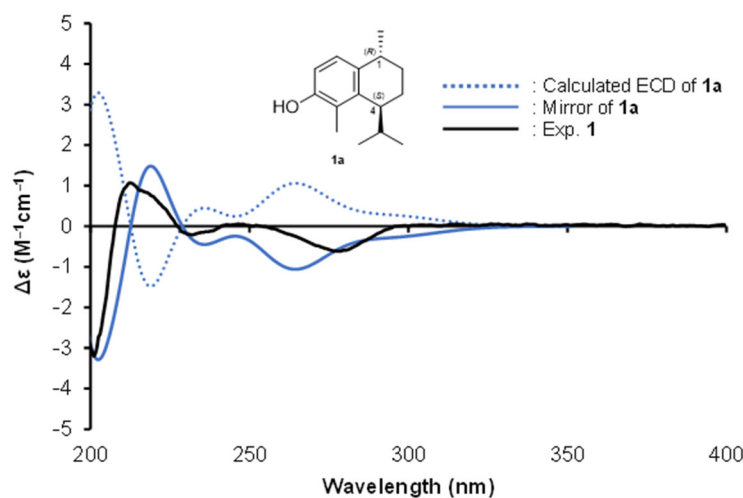


Fig 4. Calculated and experimental ECD spectra of **1a** and **1**, respectively

for a phenolic functionality. FTIR signals at 3442 cm^{-1} indicates hydroxy groups while signals at 1528 and 1475 cm^{-1} show benzene groups, confirming their incorporation into the structure. According to the ^1H - and ^{13}C -NMR spectroscopic data, compound **2** displayed analogous characteristics to compound **1** (Table 1), with the exclusive distinction being the position of phenolic hydroxyl and the quaternary aromatic methyl functionalities in the chemical structure. The HMBC correlations (Table S3 and Fig. 2) from the phenolic hydroxyl proton to C-6, C-7, and C-8 and from H₃-15 to C-5, C-6, and C-7 indicated that the phenolic hydroxyl (7-OH) and the quaternary aromatic methyl (H₃-15) groups could be at C-7 and C-6, respectively. The NOE correlations of H-8/H₃-11, H-1/H-12, and H₃-13/H-1 indicated that 1-CH₃ (C-11) and H-8 existed in the equatorial position and both 1-CH₃ and the 4-isopropyl groups revealed a *trans* relationship (Fig. 3). Compound **2** is clearly closely related to planar structures, resembling that of 5-isopropyl-3,8-dimethyl-5,6,7,8-tetrahydronaphthalen-2-ol (7-hydroxycalamenene), because its ^1H - and ^{13}C -NMR (Table 1) data were identical to those of 7-hydroxycalamenene. Additionally, the observed positive optical rotation matched exactly that of (+)-*trans*-7-methoxycalamenene ($[\alpha]_{\text{D}}^{23} +59^\circ$), which was previously isolated from cultivated *Heteroscyphus planus* liverwort cells [27].

Cytotoxic Activity

Cytotoxicity of compounds **1** and **2** against MCF-7 cells was evaluated using the resazurin reduction assay, with cisplatin as the positive control, as calculated in Fig. S23. Both inhibited cell growth, with IC₅₀ values of $196.02 \pm 0.31\ \mu\text{M}$ (**1**) and $94.44 \pm 1.42\ \mu\text{M}$ (**2**), while cisplatin, as a positive control, showed an IC₅₀ of $43.18 \pm 0.82\ \mu\text{M}$. Thus, **2** was ~2-fold more potent than **1**, though less active than cisplatin. The positioning of the C-6 methyl and C-7 hydroxyl groups on the aromatic ring may contribute to the activity observed in MCF-7 cells. Consistent with earlier reports, the sesquiterpene phenol **1** (dysoxyphenol) exhibited moderate cytotoxicity toward HL60 cells, whereas its dimer, bidysoxyphenol A, and **2** (7-hydroxycalamenene) displayed only weak effects [10-11].

In Silico Study

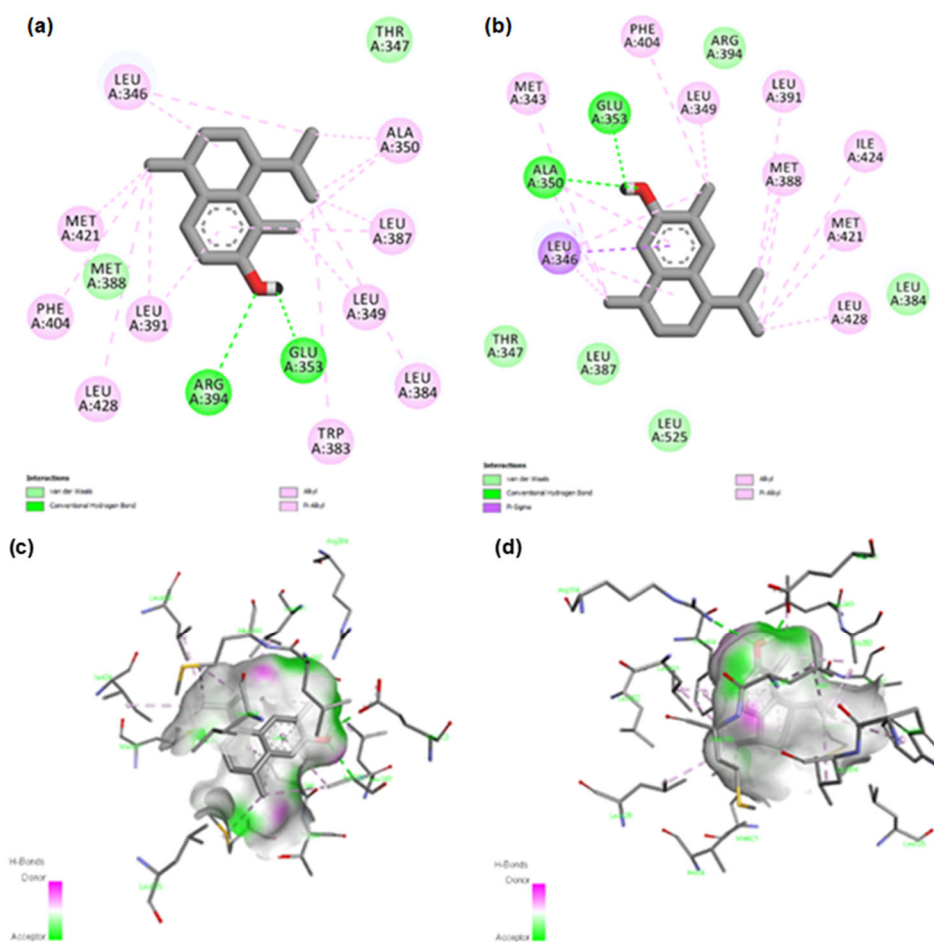
Compounds **1** and **2** are phenolic sesquiterpenes with distinct structural features that influence their interactions with target proteins [28]. The docking protocol validation was performed by redocking the native-bound ligand (OHT) into its original binding site on the estrogen receptor alpha using AutoDock 4.2, yielding an RMSD of $1.254\ \text{\AA}$, confirming acceptable accuracy. A 3D surface representation of the receptor's active site, highlighting key amino acid residues, was generated using Discovery Studio Visualizer version 2019 to better visualize ligand-protein interactions (Fig. S24; Table S4). Compound **1** contains a flexible phenolic moiety, allowing greater conformational variability and interaction potential, though this may compromise binding stability. In contrast, compound **2** has a rigid bicyclic core with a hydroxyl group at C-7, promoting hydrogen bonding while limiting flexibility.

Docking simulations showed that **1** had a slightly higher initial binding affinity for the estrogen receptor alpha (-8.03 kcal/mol) than **2** (-7.47 kcal/mol), likely due to its greater structural flexibility. However, MD simulations revealed that **2** maintained more stable interactions over time, as indicated by a lower binding free energy (-39.42 kcal/mol vs. -35.05 kcal/mol for **1**). Interaction profiles from docking are summarized in Table 2 and visualized in Fig. 5. Compound **1** exhibited paired hydrogen bonds with Glu353 and Arg394, along with multiple hydrophobic associations involving residues, including Leu346, Phe404, and Leu391. Compound **2** also formed two hydrogen bonds—one with Glu353 and another with Ala350—and engaged in extensive hydrophobic interactions, particularly with Met343, Leu346, and Met421. RMSD and RMSF analyses (Fig. 6 and 7) further supported this finding. Compound **2** exhibited lower fluctuations and more consistent binding, whereas **1** showed greater variation, particularly in flexible protein loops. Energy decomposition analysis (Fig. 8) showed that **2** benefited from stronger van der Waals and electrostatic contributions, reinforcing the role of structural rigidity in sustaining stable interactions.

Table 2. Docking results of the tested compounds. The table includes compound ID, binding energy (ΔG), predicted K_i , and types of interactions: hydrogen bonds (HB) and hydrophobic interactions (HI)

ID	ΔG (kcal/mol)	K_i (μM)	Hydrogen bond (HB)	Hydrophobic interaction (HI)
NL*	-12.01	0.00157	2 HB with Glu353 and Arg394	11 HI with Leu387, Leu391, Ala350, Met421, Leu525, Met388, Leu428, and Ile424
1	-8.03	1.30	2 HB with Glu353 and Arg394	15 HI with Leu346, Met421, Phe404, Leu391, Leu428, Trp383, Leu384, Leu349, Leu387, and Ala350
2	-7.47	3.36	2 HB with Glu353 and Ala350	14 HI with Met343, Leu346, Phe404, Leu349, Leu391, Met388, Ile424, Met421, and Leu428

* NL = native ligand (4-hydroxytamoxifen, OHT)

**Fig 5.** The (a) 2D and (c) 3D binding interactions for compound 1, and the (b) 2D and (d) 3D binding interactions for compound 2 are presented, respectively. After molecular docking using AutoDock 4.2, the interactions between each compound and the active site of the estrogen receptor alpha were visualized in 2D and 3D. Hydrogen bonds are shown as green dashed lines, highlighting key interactions that help stabilize the binding. Hydrophobic contacts and other relevant interactions are also illustrated to show how each compound fits within the binding pocket

In cytotoxicity assays, both compounds showed promising activity against MCF-7 breast cancer cells. Notably, compound 2 was more potent ($IC_{50} = 94.44 \mu M$)

than compound 1 ($IC_{50} = 196.02 \mu M$) and even outperformed the standard drug cisplatin ($IC_{50} = 43.18 \mu M$). This enhanced activity may be attributed to

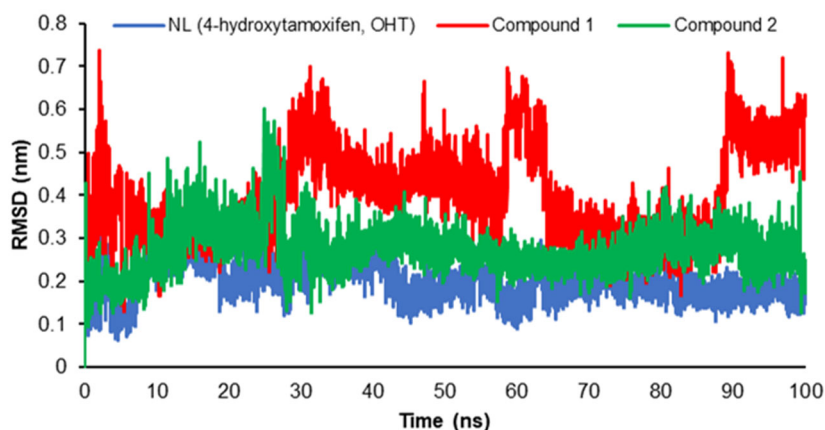


Fig 6. RMSD of the native ligand (NL; OHT; blue), compound 1 (red), and 2 (green) bound to the estrogen receptor alpha. A 100-ns simulation was run using GROMACS to check the stability of each compound bound to the protein. Lower and steady RMSD values indicate more stable binding

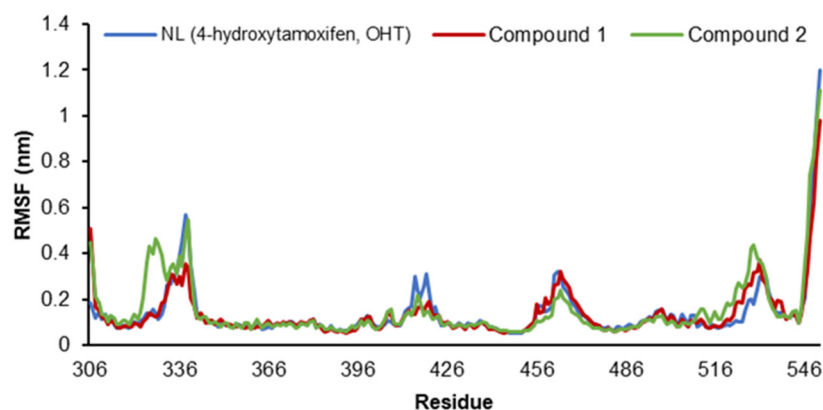


Fig 7. RMSF values for the native ligand (NL; OHT; blue), compound 1 (red), and compound 2 (green) bound to the estrogen receptor alpha target. A 100-nanosecond MD simulation was performed using GROMACS to analyze the flexibility of protein residues when bound to each compound. RMSF measures how much each part of the protein moves during the simulation, helping to identify regions affected by ligand binding

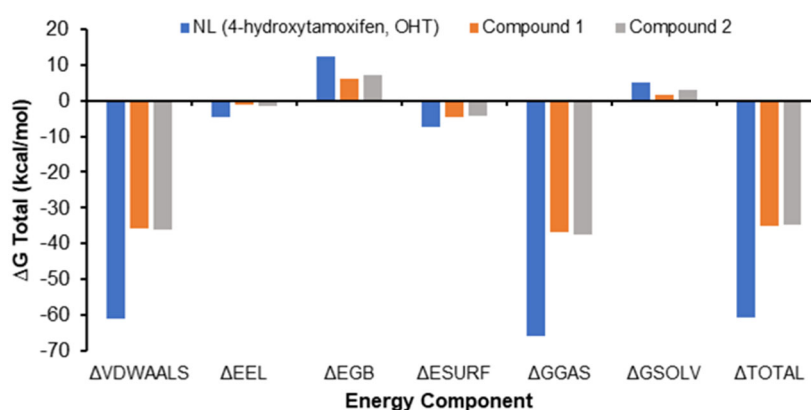


Fig 8. Energy components of the native ligand (NL; OHT), compounds 1 and 2 when bound to the estrogen receptor alpha target. Binding energy components were calculated to understand the contributions of different forces—such as van der Waals, electrostatic, and solvation energies—using molecular mechanics calculations. This analysis helps reveal how each compound interacts with the protein and contributes to the overall binding strength

the C-7 hydroxyl and the C-6 methyl groups, which are known to enhance cellular interactions and cytotoxic responses [29]. The higher inhibitory concentration values indicated that these compounds required higher concentrations to achieve the same cytotoxic effect as cisplatin, suggesting lower overall potency. Nevertheless, molecular docking studies revealed that both compounds formed interactions similar to those of the native ligand. Compounds **1** and **2** engaged in hydrogen bonding with key estrogen receptor residues, particularly Glu353 and Arg394, which are crucial for ligand recognition and receptor stabilization [30-31]. Additionally, they exhibited extensive hydrophobic interactions with residues such as Leu391, Met421, and Leu428, resembling the interaction profile of NL. Although their binding affinities ($\Delta G = -8.03$ and -7.47 kcal/mol for compounds **1** and **2**, respectively) were weaker than that of NL (-12.01 kcal/mol), the higher number of hydrophobic contacts might contribute to favorable receptor accommodation and improved molecular stability. These interaction patterns suggested that, despite their lower cytotoxic potency, compounds **1** and **2** exhibited a binding mode comparable to that of the standard ligand and could serve as structural leads for further optimization to enhance estrogen receptor affinity and anticancer activity. These results align with previous studies highlighting the importance of molecular rigidity, hydroxyl substitution, and stable hydrogen bonding in enhancing the anticancer potential of phenolic compounds targeting estrogen receptors [32]. McCullough et al. demonstrated that hydroxylated phenolics can interact effectively with estrogen receptor alpha (ER α) via hydrogen bonding, particularly with Arg394 and Glu353, similar to the natural estrogen 17 β -estradiol [33]. Feng et al. reported that rigid molecular frameworks promote more stable binding by reducing conformational fluctuations [34]. Meanwhile, Rajalakshmi et al. further confirmed through QSAR analysis that appropriately substituted phenolic compounds exhibit stronger ER-binding affinity and cytotoxic activity [35]. Altogether, these *in vitro* and *in silico* findings suggest that compound **2** has greater therapeutic potential as a lead compound for estrogen receptor-targeted anticancer therapy.

In docking simulations, compound **1** showed a slightly better binding affinity to the estrogen receptor alpha (-8.03 kcal/mol) than compound **2** (-7.47 kcal/mol), suggesting that its flexibility facilitates favorable initial binding (Table 2). However, MD simulations revealed a different trend—compound **2** demonstrated greater conformational stability and a more favorable binding energy (-39.42 kcal/mol) compared to compound **1** (-35.05 kcal/mol), indicating more stable interactions over time.

The dynamic behavior of each ligand-protein complex was evaluated through RMSD and RMSF plots (Fig. 6 and 7). Compound **2** maintained more consistent binding with lower RMSD variation, while compound **1** exhibited slightly higher fluctuations due to its flexible structure. RMSF analysis highlighted specific residue regions affected by ligand binding, especially in compound **1**, which led to greater fluctuations in flexible protein loops. Additionally, energy decomposition analysis (Fig. 8) provided insight into the forces driving binding affinity. Compound **2** exhibited stronger van der Waals and electrostatic interactions, consistent with the observation that rigidity favors sustained interactions within the binding site. These findings demonstrate the complementary value of docking and MD simulations: docking captures initial binding affinity, while MD elucidates the long-term stability and adaptability of the ligands in a dynamic environment.

The cytotoxic assay results revealed that both **1** and **2** exhibited promising activity against MCF-7 cells. Notably, **2** demonstrated greater cytotoxicity than **1**. This enhanced activity may be attributed to the presence of methyl and hydroxyl groups at the C-6 and C-7 positions, respectively, on the aromatic ring, which are known to influence interactions with cellular targets and enhance cytotoxicity.

These biological findings are well supported by *in silico* molecular interaction studies. Although molecular docking initially suggested that compound **1** had a slightly better binding affinity to the estrogen receptor alpha at -8.03 kcal/mol compared to -7.47 kcal/mol for compound **2**, further MD simulations revealed a more nuanced picture. Over the course of the simulation,

compound **2** maintained a more stable interaction, with a significantly lower binding free energy (-39.42 kcal/mol) compared to compound **1** (-35.05 kcal/mol). This indicates that while compound **1** may form more flexible initial contacts, compound **2** offers a more robust and persistent engagement with the receptor site.

This stability was further supported by RMSD and RMSF analyses. Compound **2** showed lower fluctuations during the simulation, suggesting a more consistent interaction, likely due to its rigid bicyclic structure and the strategic placement of its hydroxyl group, which facilitates stable hydrogen bonding. In contrast, the flexible phenolic structure of compound **1** led to greater conformational variability, particularly in the protein's flexible loop regions. Additionally, energy decomposition analysis revealed that compound **2** benefited from stronger van der Waals and electrostatic interactions—key factors in maintaining long-term binding stability [36].

The complementary nature of these computational methods is clearly demonstrated: docking helps predict initial binding preferences, while MD simulations provide insight into how well the ligand–protein complex holds together over time. When these findings are considered alongside the cytotoxicity data, it becomes evident that the superior biological activity of compound **2** is likely due to its favorable, stable interaction with the estrogen receptor, supporting its potential as a lead compound for further development.

These findings are consistent with earlier studies that emphasize the importance of structural features, particularly molecular rigidity, hydroxyl substitution, and stable hydrogen-bonding networks, in enhancing the anticancer potential of phenolic compounds targeting estrogen receptors. Previous research demonstrated that phenolic compounds containing hydroxyl groups can effectively interact with estrogen receptor alpha (ER α) through hydrogen bonding, especially with residues Arg394 and Glu353, in a manner similar to the natural ligand 17 β -estradiol [33]. Similarly, phenolic compounds with rigid frameworks exhibit more stable binding within the ER binding pocket due to reduced conformational flexibility, which facilitates consistent hydrogen bonding and van der Waals interactions [37]. Furthermore, Hu

and Aizawa [38] demonstrated, through a QSAR study, that phenolics with optimally positioned hydroxyl groups and favorable molecular properties tend to exhibit higher ER-binding affinity and stronger cytotoxic effects. Collectively, these findings support the current study and highlight the critical influence of specific structural characteristics on the bioactivity of phenolic ligands against estrogen receptors.

■ CONCLUSION

In conclusion, two sesquiterpenes were isolated from *D. parasiticum* leaves and identified as dysoxyphenol (**1**) and 7-hydroxycalamenene (**2**) based on spectroscopy and specific optical rotation, and ECD analysis data. Both compounds showed potent cytotoxicity against MCF-7 cells. Molecular interaction studies revealed that **1**, with its more flexible molecular structure, exhibited stronger binding interactions in the initial molecular docking simulations. Conversely, the more rigid framework of **2** proved advantageous in molecular dynamics simulations, resulting in more stable and energetically favorable ligand–receptor interactions over time. Among them, compound **2** demonstrated slightly better binding stability and interaction profiles. These findings suggest that both compounds have promising anticancer potential.

■ ACKNOWLEDGMENTS

The authors express their gratitude to Prof. Takako Aboshi and Prof. Hiroyuki Konno from Yamagata University for their assistance with the HR-ESI TOF-MS and ECD experiments, respectively. The first author and Unang Supratman gratefully acknowledge financial support from Universitas Padjadjaran, Indonesia, for the Senior Lecturer Acceleration Research Grant (number: 1623/UN6.3.1/PT.00/2024) and the Academic Leadership Grant (number: 1630/UN6.3.1/PT.00/2024) in 2024, respectively.

■ CONFLICT OF INTEREST

The authors declare no conflicts of interest.

■ AUTHOR CONTRIBUTIONS

Ferry Ferdiansyah Sofian and Unang Supratman

wrote and revised the manuscript. Amrina Virliana and Ahda Salsabila Izzaturrahmi conducted the isolation experiment; Ellin Febrina and Aiyi Asnawi conducted the molecular study; Tjandrawati Mozef conducted the cytotoxicity experiment; Kindi Farabi and Eri Bachtiar conducted the spectral data analyses; Nurlelasari conducted project administration; Anas Subarnas and Yasmiwar Susilawati conducted supervision; and Yoshihito Shiono conducted the DFT calculations and supervision. All authors approved the final version of this article.

■ REFERENCES

- [1] Newman, D.J., and Cragg, G.M., 2020, Natural products as sources of new drugs over the nearly four decades from 01/1981 to 09/2019, *J. Nat. Prod.*, 83 (3), 770–803.
- [2] Atanasov, A.G., Zotchev, S.B., Dirsch, V.M., Orhan, I.E., Banach, M., Rollinger, J.M., Barreca, D., Weckwerth, W., Bauer, R., Bayer, E.A., Majeed, M., Bishayee, A., Bochkov, V., Bonn, G.K., Braid, N., Bucar, F., Cifuentes, A., D'Onofrio, G., Bodkin, M., Diederich, M., Dinkova-Kostova, A.T., Efferth, T., El Bairi, K., Arkells, N., Fan, T.P., Fiebich, B.L., Freissmuth, M., Georgiev, M.I., Gibbons, S., Godfrey, K.M., Gruber, C.W., Heer, J., Huber, L.A., Ibanez, E., Kijjoo, A., Kiss, A.K., Lu, A., Macias, F.A., Miller, M.J.S., Mocan, A., Müller, R., Nicoletti, F., Perry, G., Pittalà, V., Rastrelli, L., Ristow, M., Russo, G.L., Silva, A.S., Schuster, D., Sheridan, H., Skalicka-Woźniak, K., Skaltsounis, L., Sobarzo-Sánchez, E., Bredt, D.S., Stuppner, H., Sureda, A., Tzvetkov, N.T., Vacca, R.A., Aggarwal, B.B., Battino, M., Giampieri, F., Wink, M., Wolfender, J.L., Xiao, J., Yeung, A.W.K., Lizard, G., Popp, M.A., Heinrich, M., Berindan-Neagoe, I., Stadler, M., Daglia, M., Verpoorte, R., and Supuran, C.T., 2021, Natural products in drug discovery: Advances and opportunities, *Nat. Rev. Drug Discovery*, 20 (3), 200–216.
- [3] Kew Royal Botanic Gardens, 2023, *Dysoxylum parasiticum* (Osbeck) Kosterm, <https://powo.science.kew.org/taxon/urn:lsid:ipni.org:names:578268-1>, accessed on February 22, 2024.
- [4] Tsuji, Y., Mitani, M., Widayanti, K.A., Suryobroto, B., and Watanabe, K., 2019, Dietary habits of wild Javan lutungs (*Trachypithecus auratus*) in a secondary-plantation mixed forest: Effects of vegetation composition and phenology, *Mamm. Biol.*, 98, 80–90.
- [5] Fauzi, A., Suwandhi, I., and Suhaya, Y., 2025, Habitat suitability of Javan langur (*Trachypithecus auratus*) in Gunung Babakan, West Java, Indonesia, *Biodiversitas*, 26 (8), 3815–3826.
- [6] Petroni, L.M., Huffman, M.A., and Rodrigues, E., 2017, Medicinal plants in the diet of woolly spider monkeys (*Brachyteles arachnoides*, E. Geoffroy, 1806) – A bio-rational for the search of new medicines for human use?, *Rev. Bras. Farmacogn.*, 27 (2), 135–142.
- [7] Abdullah, R., Milanda, T., Sugijanto, M., Barliana, M.I., Diantini, A., Supratman, U., and Subarnas, A., 2017, Antibacterial properties of selected plants consumed by primates against *Escherichia coli* and *Bacillus subtilis*, *Southeast Asian J. Trop. Med. Public Health*, 48 (1), 109–116.
- [8] Arief, N.R., Sofian, F.F., Aboshi, T., Kuncoro, H., Dinata, D.I., Shiono, Y., and Nishikawa, Y., 2024, Evaluation of the antiplasmodial and anti-toxoplasma activities of several Indonesian medicinal plant extracts, *J. Ethnopharmacol.*, 331, 118269.
- [9] Naini, A.A., Mayanti, T., Harneti, D., Darwati, D., Nurlelasari, N., Maharani, R., Farabi, K., Herlina, T., Supratman, U., Fajriah, S., Kuncoro, H., Azmi, M.N., Shiono, Y., Jungsuttiwong, S., and Chakthong, S., 2023, Sesquiterpenoids and sesquiterpenoid dimers from the stem bark of *Dysoxylum parasiticum* (Osbeck) Kosterm, *Phytochemistry*, 205, 113477.
- [10] Sofian, F.F., Subarnas, A., Hakozaki, M., Uesugi, S., Koseki, T., and Shiono, Y., 2022, Tridysoxyphenols A and B, two new trimeric sesquiterpene phenols from *Dysoxylum parasiticum* leaves, *Phytochem. Lett.*, 50, 134–140.
- [11] Sofian, F.F., Subarnas, A., Hakozaki, M., Uesugi, S., Koseki, T., and Shiono, Y., 2022, Bidysoxyphenols A–C, dimeric sesquiterpene phenols from the

- leaves of *Dysoxylum parasiticum* (Osbeck) Kosterm, *Fitoterapia*, 158, 105157.
- [12] Naini, A.A., Mayanti, T., Maharani, R., Harneti, D., Nurlelasari, N., Farabi, K., Fajriah, S., Hilmayanti, E., Kabayama, K., Shimoyama, A., Manabe, Y., Fukase, K., Jungstutiwong, S., Prescott, T.A.K., and Supratman, U., 2024, Paraxylines A-G: Highly oxygenated preurianin-type limonoids with immunomodulatory TLR4 and cytotoxic activities from the stem bark of *Dysoxylum parasiticum*, *Phytochemistry*, 220, 114009.
- [13] Wibawa, I.P.A.H., Hermawan, F., Minarti, M., Lotulung, P.D., Artanti, N., Hanafi, M., Butardo, V.M., and Mahon, P.J., 2025, Novel trinorditerpene from *Dysoxylum parasiticum* (Osbeck) Kosterm: Leaf extract with cytotoxic, antioxidant and α -glucosidase inhibitory activities, *Molecules*, 30 (24), 4747.
- [14] Frisch, M.J., Trucks, G.W., Schlegel, H.B., Scuseria, G.E., Robb, M.A., Cheeseman, J.R., Scalmani, G., Barone, V., Mennucci, B., Petersson, G.A., Nakatsuji, H., Caricato, M., Li, X., Hratchian, H.P., Izmaylov, A.F., Bloino, J., Zheng, G., Sonnenberg, J.L., Hada, M., Ehara, M., Toyota, K., Fukuda, R., Hasegawa, J., Ishida, M., Nakajima, T., Honda, Y., Kitao, O., Nakai, H., Vreven, T., Montgomery, J.A., Jr., Peralta, J.E., Ogliaro, F., Bearpark, M., Heyd, J.J., Brothers, E., Kudin, K.N., Staroverov, V.N., Kobayashi, R., Normand, J., Raghavachari, K., Rendell, A., Burant, J.C., Iyengar, S.S., Tomasi, J., Cossi, M., Rega, N., Millam, J.M., Klene, M., Knox, J.E., Cross, J.B., Bakken, V., Adamo, C., Jaramillo, J., Gomperts, R., Stratmann, R.E., Yazyev, O., Austin, A.J., Cammi, R., Pomelli, C., Ochterski, J.W., Martin, R.L., Morokuma, K., Zakrzewski, V.G., Voth, G.A., Salvador, P., Dannenberg, J.J., Dapprich, S., Daniels, A.D., Farkas, Ö., Foresman, J.B., Ortiz, J.V., Cioslowski, J., and Fox, D.J., 2013, *Gaussian-09 Revision D.01*, Gaussian, Inc., Wallingford, CT.
- [15] Blum, V., Asahi, R., Autschbach, J., Bannwarth, C., Bihlmayer, G., Blügel, S., Burns, L.A., Crawford, T.D., Dawson, W., de Jong, W.A., Draxl, C., Filippi, C., Genovese, L., Giannozzi, P., Govind, N., Hammes-Schiffer, S., Hammond, J.R., Hourahine, B., Jain, A., Kanai, Y., Kent, P.R.C., Larsen, A.H., Lehtola, S., Li, X., Lindh, R., Maeda, S., Makri, N., Moussa, J., Nakajima, T., Nash, J.A., Oliveira, M.J.T., Patel, P.D., Pizzi, G., Pourtois, G., Pritchard, B.P., Rabani, E., Reiher, M., Reining, L., Ren, X., Rossi, M., Schlegel, H.B., Seriani, N., Slipchenko, L.V., Thom, A., Valeev, E.F., Van Troeye, B., Visscher, L., Vlček, V., Werner, H.J., Williams-Young, D.B., and Windus, T.L., 2024, Roadmap on methods and software for electronic structure based simulations in chemistry and materials, *Electron. Struct.*, 6 (4), 042501.
- [16] Li, Z., Jiang, M., Wang, S., and Zhang, S., 2022, Deep learning methods for molecular representation and property prediction, *Drug Discovery Today*, 27 (12), 103373.
- [17] Renj, D.P.L., Geetha, R.R.J., Benifa, A., Amalanathan, M., Mary, M.S.M., Ratkovic, Z., Muškinja, J., and Micheal, J., 2024, Density functional theory calculations, vibrational spectral analysis and topological analysis of 1-acethyl-2(4-isopropoxy-3-methoxyphenyl) cyclopropane with docking studies, *Chem. Phys. Impact*, 8, 100524.
- [18] Sánchez-Díez, M., Romero-Jiménez, P., Alegría-Aravena, N., Gavira-O'Neill, C.E., Vicente-García, E., Quiroz-Troncoso, J., González-Martos, R., Ramírez-Castillejo, C., and Pastor, J.M., 2025, Assessment of cell viability in drug therapy: IC₅₀ and other new time-independent indices for evaluating chemotherapy efficacy, *Pharmaceutics*, 17 (2), 247.
- [19] Snyder, H.D., and Kucukkal, T.G.K., 2021, Computational chemistry activities with Avogadro and ORCA, *J. Chem. Educ.*, 98 (4), 1335–1341.
- [20] Shaimardanov, A.R., Shulga, D.A., and Palyulin, V.A., 2022, Is an inductive effect explicit account required for atomic charges aimed at use within the force fields?, *J. Phys. Chem. A*, 126 (36), 6278–6294.
- [21] Butt, S.S., Badshah, Y., Shabbir, M., and Rafiq, M., 2020, Molecular docking using Chimera and Autodock Vina software for nonbioinformaticians, *JMIR Bioinf. Biotechnol.*, 1 (1), e14232.

- [22] Febrina, E., Asnawi, A., Abdulah, R., Lestari, K., and Supratman, U., 2022, Identification of flavonoids from *Acalypha indica* L. (Euphorbiaceae) as caspase-3 activators using molecular docking and molecular dynamics, *Int. J. Appl. Pharm.*, 14 (5), 162–166.
- [23] Abbas, R.F., and Farhan, M.S., 2025, Synthesis and antibacterial evaluation of novel ketoprofen derivatives as bacterial transpeptidase inhibitors via combined *in silico* and *in vitro* approaches, *Indones. J. Chem.*, 25 (6), 1930–1943.
- [24] Kutzner, C., Kniep, C., Cherian, A., Nordstrom, L., Grubmüller, H., de Groot, B.L., and Gapsys, V., 2022, GROMACS in the cloud: A global supercomputer to speed up alchemical drug design, *J. Chem. Inf. Model.*, 62 (7), 1691–1711.
- [25] Jejurikar, B.L., and Rohane, S.H., 2021, Drug designing in discovery studio, *Asian J. Res. Chem.*, 14 (2), 135–138.
- [26] Dharmayani, N.K.T., Yoshimura, T., Hermawati, E., Juliawaty, L.D., and Syah, Y.M., 2019, Antibacterial and antifungal two phenolic sesquiterpenes from *Dysoxylum densiflorum*, *Z. Naturforsch., C: Biosci.*, 75 (1-2), 1–5.
- [27] Nabeta, K., Katayama, K., Nakagawara, S., and Katoh, K., 1992, Sesquiterpenes of cadinane type from cultured cells of the liverwort, *Heteroscyphus planus*, *Phytochemistry*, 32 (1), 117–122.
- [28] Hilal, B., Khan, M.M., and Fariduddin, Q., 2024, Recent advancements in deciphering the therapeutic properties of plant secondary metabolites: Phenolics, terpenes, and alkaloids, *Plant Physiol. Biochem.*, 211, 108674.
- [29] Ramuthai, M., Jeyavijayan, S., Premkumar, R., Priya, M.U., and Jayram, N.D., 2022, Structure, spectroscopic investigation, molecular docking and *in vitro* cytotoxicity studies on 4,7-dihydroxycoumarin: A breast cancer drug, *J. Comput. Biophys. Chem.*, 21 (2), 219–236.
- [30] Rej, R.K., Thomas II, J.E., Acharyya, R.K., Rae, J.M., and Wang, S., 2023, Targeting the estrogen receptor for the treatment of breast cancer: Recent advances and challenges, *J. Med. Chem.*, 66 (13), 8339–8381.
- [31] Dai, Y.H., Chen, G.Y., Tang, C.H., Huang, W.C., Yang, J.C., and Wu, Y.C., 2021, Drug screening of potential multiple target inhibitors for estrogen receptor- α -positive breast cancer, *In Vivo*, 35 (2), 761–777.
- [32] Xiang, Y., Xiang, M., Mao, Y., Huang, L., He, Q., and Dong, Y., 2025, Insights into structure-antioxidant activity relationships of polyphenol-phospholipid complexes: The effect of hydrogen bonds formed by phenolic hydroxyl groups, *Food Chem.*, 485, 144471.
- [33] McCullough, C., Neumann, T.S., Gone, J.R., He, Z., Herrild, C., Wondergem (nee Lukesh), J., Pandey, R.K., Donaldson, W.A., and Sem, D.S., 2014, Probing the human estrogen receptor- α binding requirements for phenolic mono- and di-hydroxyl compounds: A combined synthesis, binding and docking study, *Bioorg. Med. Chem.*, 22 (1), 303–310.
- [34] Feng, L., Astumian, R.D., and Stoddart, J.F., 2022, Controlling dynamics in extended molecular frameworks, *Nat. Rev. Chem.*, 6 (10), 705–725.
- [35] Rajalakshmi, P., Peter, D.N., Johnson, S.J., and Ananthi, N., 2021, Structure-activity relationship of supramolecular compounds in drug delivery, *Mini-Rev. Org. Chem.*, 18 (7), 961–989.
- [36] Mao, Y., Loipersberger, M., Horn, P.R., Das, A., Demerdash, O., Levine, D.S., Prasad Veccham, S., Head-Gordon, T., and Head-Gordon, M., 2021, From intermolecular interaction energies and observable shifts to component contributions and back again: A tale of variational energy decomposition analysis, *Annu. Rev. Phys. Chem.*, 72, 641–666.
- [37] Tabira, Y., Nakai, M., Asai, D., Yakabe, Y., Tahara, Y., Shinmyozu, T., Noguchi, M., Takatsuki, M., and Shimohigashi, Y., 1999, Structural requirements of para-alkylphenols to bind to estrogen receptor, *Eur. J. Biochem.*, 262 (1), 240–245.
- [38] Hu, J.Y., and Aizawa, T., 2003, Quantitative structure-activity relationships for estrogen receptor binding affinity of phenolic chemicals, *Water Res.*, 37 (6), 1213–1222.